Palladium diffusion into bulk copper via the (100) surface

2009 J. Phys.: Condens. Matter 21 314016

(http://iopscience.iop.org/0953-8984/21/31/314016)

J. Phys.: Condens. Matter **21** (2009) 314016 (7pp) doi:10.1088/0953-8984/21/31/314016

Palladium diffusion into bulk copper via the (100) surface

E Bussmann[1], J Sun[2,3], K Pohl[2] and G L Kellogg[1]

[1] Sandia National Laboratories, Albuquerque, NM 87185, USA
[2] Department of Physics and Materials Science Program, University of New Hampshire, Durham, NH 03824, USA

Received 31 December 2008, in final form 2 April 2009
Published 7 July 2009
Online at stacks.iop.org/JPhysCM/21/314016

Abstract
Using low-energy electron microscopy, we measure the diffusion of Pd into bulk Cu at the Cu(100) surface. Interdiffusion is tracked by measuring the dissolution of the Cu(100)–c(2 × 2)-Pd *surface alloy* during annealing ($T > 240\,^{\circ}$C). The activation barrier for Pd diffusion from the surface alloy into the bulk is determined to be (1.8 ± 0.6) eV. During annealing, we observe the growth of a new layer of Cu near step edges. Under this new Cu layer, dilute Pd remaining near the surface develops a layered structure similar to the Cu_3Pd $L1_2$ bulk alloy phase.

(Some figures in this article are in colour only in the electronic version)

1. Introduction

Binary alloy thin films of Pd and Cu have attractive properties for a variety of technological applications [1, 2]. Owing to Pd's ability to dissociatively adsorb H_2, Pd–Cu alloy thin films are useful in catalysis, e.g. to promote water–gas shift reactions as in hydrogen purification [2]. In microelectronics, Pd–Cu alloys may be used to make components, e.g. interconnects, less susceptible to electromigration damage [3–5]. In such applications, *ultrathin* Pd–Cu alloy films are of interest, e.g. as electromigration-resistant surface coatings or gas-permeable membranes. At the Cu(100) surface, submonolayer coverages of Pd form *surface or interfacial* alloys, involving only the two or three outermost atomic planes [1, 6–13]. Besides providing a model system to study the growth of alloy thin films, we have found that the surface alloy slows the surface diffusion process [5], which limits the rate of electromigration in sub-micrometer-wide Cu wires [3]. Since Pd and Cu are bulk miscible, the surface alloy is unstable at temperatures sufficient for Pd interdiffusion into bulk Cu. Previous studies of the interdiffusion of Pd into Cu have explored the process on macroscopic length scales with 'cook-and-look' techniques [14–17]. To our knowledge, previous studies have not examined the stability of the surface alloy and the early stages of the interdiffusion process. In this work, we use low-energy electron microscopy (LEEM) to characterize the temperature-dependent dissolution of the surface alloy into the Cu bulk. The LEEM enables us to observe the interdiffusion and the evolution of the near-surface structure at the nanometer scale in real-time.

In the temperature range of our experiments ($T > 150\,^{\circ}$C), submonolayer coverages of Pd form a *buried* surface alloy at the Cu(100) surface [1, 6–13]. The structure and growth of the buried surface alloy are well understood [6–13]. On terraces, figure 1(a), the buried alloy consists of a c(2 × 2)-ordered Pd–Cu underlayer covered by a monolayer of nearly pure Cu [11–13]. Near step edges, Hannon *et al* found that some Pd is also present in the third atomic layer, as shown in figure 1(b). Hannon *et al* explained that this structure originates from step flow during the growth of the alloy [12]. As Pd adsorbed onto the terrace is incorporated into the second atomic layer, Cu is displaced to the surface. The displaced Cu migrates to nearby steps, causing the steps to advance. The advancing steps grow over the buried alloy on the terrace, so that some Pd then resides in the third atomic layer. On the upper side of the step, arriving Pd continues to be incorporated into the second layer as well, leading to Pd in both the second and third layers.

The buried surface alloy is intrinsically thermally metastable; increasing Pd–Cu coordination lowers the configurational energy of the system [12, 13] and mixing of Pd into the Cu bulk is favored entropically. In this work, we use LEEM to characterize this inherent thermal instability by directly imaging the dissolution of the buried surface alloy

[3] Present address: IBM Research Division, T J Watson Research Center, Yorktown Heights, NY 10598, USA.

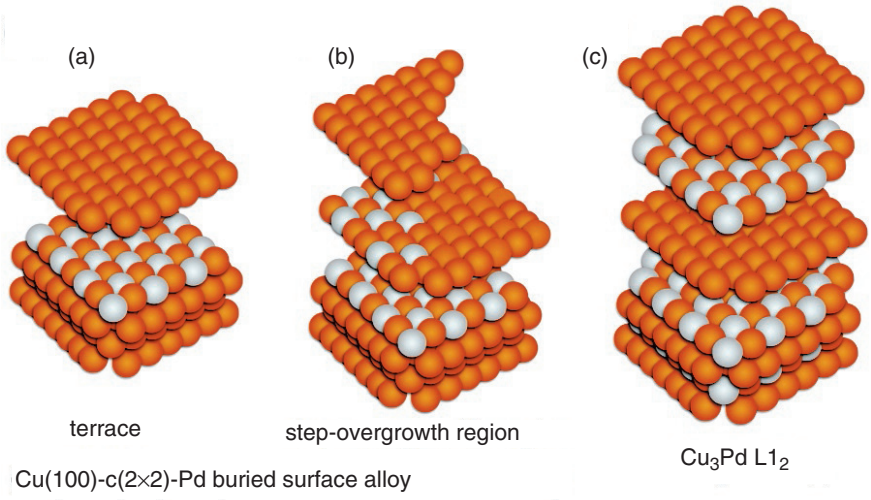

Figure 1. Schematic structures of the Cu(100)–c(2 × 2)-Pd buried surface alloy and the bulk Cu_3Pd $L1_2$ structure. (a) On terraces, Pd is buried in the second atomic layer, covered by a nearly pure layer of Cu. (b) Step-overgrowth regions, where Pd is buried in the second and third atomic layers, near step edges. (c) A schematic of the ordered Cu_3Pd $L1_2$ alloy phase which occurs for $T < 370\,^{\circ}C$ in Pd–Cu bulk alloys with less than 21 at.% Pd.

while annealing our samples ($T > 240\,^{\circ}C$). During the annealing period, we observe that the terraces, figure 1(a), and step-edge regions, figure 1(b), evolve along different pathways. On terraces, Pd diffuses into the Cu bulk from the outset of the annealing process. Using LEEM intensity versus voltage (I–V) measurements [12, 13], we track the interdiffusion and estimate the Pd diffusion rates at several temperatures. We obtain an activation barrier of (1.8 ± 0.6) eV for Pd diffusion in Cu. In the step-edge region, we observe the nucleation and growth of a new layer of Cu during the annealing period. A LEEM I–V analysis shows that, under this new Cu layer, the Pd near the surface is reorganized into a layered structure similar to the Cu_3Pd $L1_2$ bulk alloy shown in figure 1(c) [1, 18]. Over time, this Cu_3Pd $L1_2$ structure becomes dilute. The complete dissolution of the surface alloy into the Cu bulk is the ultimate outcome of annealing over long times.

2. Methods and materials

2.1. LEEM I–V technique and analysis

We characterize the evolution of the near-surface structure using LEEM I–V measurements in combination with dynamical LEED I–V analysis [12, 13]. LEEM I–V measurements are analogous to low-energy electron diffraction (LEED) I–V measurements, a well-established technique for surface structural characterization [19]. In a LEEM I–V measurement, the intensity of electrons reflected from the surface is recorded as a function of their kinetic energy. Specifically, a sequence of LEEM images is recorded while incrementally varying the electron kinetic energy. An aperture is placed in the backfocal (diffraction) plane so that only electrons in the specular beam are recorded in the image. The specular electron reflectivity is dependent on the electron kinetic energy and also on the structure of the surface to a depth of several atomic layers [12, 13].

The structure and composition of the outermost atomic layers are determined from the LEEM I–V data by a dynamical LEED I–V analysis [13]. Previously, Hannon *et al* used this method to reveal the terrace and step-overgrowth structure of the buried alloy grown under the same conditions as in our present work, see figures 1(a) and (b) [12]. In the I–V analysis, multiple-scattering theory is used to calculate the reflectivity versus energy relationship for a trial surface structure. Then the calculated curves are compared with experiment. By an iterative process, key structural parameters, e.g. Pd concentrations in the outermost three, or four, atomic layers of the trial structure, are optimized to give the best agreement between the calculated and experimental I–V curves[4]. Two recent publications give the details of our implementation of I–V analysis, with a complete list of the structural parameters that are optimized [12, 13].

2.2. Materials and preparation

Our experiments are performed in an ELMITEC LEEM III system at pressures below 5×10^{-10} Torr. We perform experiments on a single-crystal Cu (99.999%) sample cut and electropolished to within about 0.1° of the [100] azimuth. Prior to experiments, the sample is annealed in a furnace at 900 °C under an atmosphere of Ar4%H_2 for 24 h to deplete sulfur and carbon contamination. The sample surface is cleaned by numerous cycles of 1 keV Ar^+ or Ne^+ ion sputtering interleaved with annealing at 700–800 °C. When the sample is sufficiently clean to see the step-terrace structure in LEEM images, the surface is further prepared by sublimation (∼850 °C) of several atomic layers of Cu from the surface. The flow of monatomic surface steps during sublimation is

[4] The criterion by which we determine uncertainties in C_i is explained in [13].

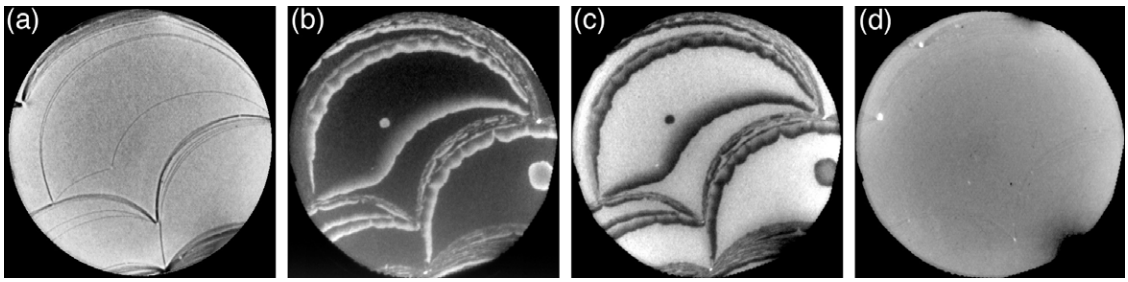

Figure 2. (a) A LEEM image of the clean Cu surface (2 eV electron energy). ((b), (c)) Images of the c(2 × 2)-Pd buried surface alloy (0.4 ML Pd) acquired with electron energies of 14.5 eV (b) and 20.1 eV (c), respectively. (d) A 14.5 eV image of the alloy surface after annealing at 370 °C for 10 min does not show the contrast observed in image (b), taken prior to annealing. FOV = 5 μm.

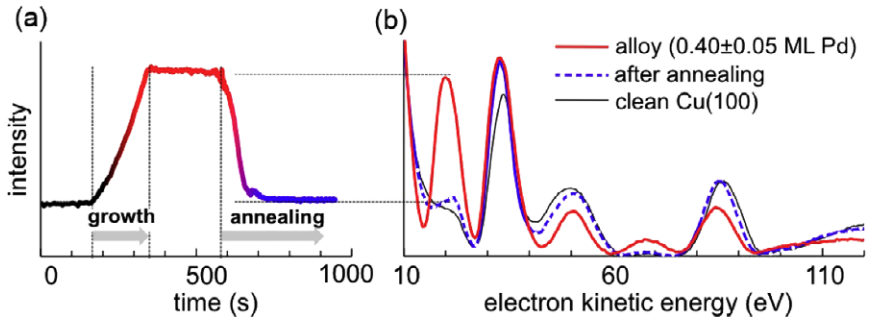

Figure 3. (a) The timeline of an experiment showing how the intensity of reflected 20.3 eV electrons is used to track the buried alloy growth and dissolution during annealing. (b) I–V curves showing the energy-dependent reflectivity for a clean Cu(100) terrace, the terrace after growth of a 0.4 ML Pd alloy and the alloy terrace after annealing at 370 °C for 10 min.

observed by LEEM. Smooth, unimpeded step flow is taken as an indication of acceptable surface cleanliness. Figure 2(a) shows a LEEM image, with atomic-step contrast, of the clean Cu(100) surface acquired with an electron energy of 2 eV. Individual atomic steps and step bunches are evident.

To prepare the buried surface alloy, Pd is deposited at ∼5 ML h^{-1} from an e-beam-heated Pd wire source onto the sample held at 200–220 °C. Temperatures are measured by a type-C thermocouple spot-welded to a molybdenum ring, which is pressed against the back of the sample. The Pd deposition rate is calibrated by measuring the intensity of the half-order LEED spots associated with the c(2 × 2)-Pd structure, which is known to reach a maximum near 0.55 ML Pd coverage [6].

3. Palladium diffusion into the Cu(100) surface

3.1. Thermal instability of the surface alloy

Figures 2(b) and (c) show specular LEEM images of the buried surface alloy containing 0.4 ML Pd. The contrast in the images is due to the structural and compositional variation arising from the step-overgrowth mechanism observed by Hannon *et al* [12, 13]. In figure 2(b) at 14.5 eV, terrace regions, containing primarily second-layer Pd as in figure 1(a), appear dark. The brighter regions near step edges contain Pd in both the second and third atomic layers, as in figure 1(b), due to the step-overgrowth mechanism. In figure 2(c), at 20.1 eV, the bright–dark contrast is inverted. The energy-dependent bright–dark contrast of the surface alloy completely vanishes, as shown in figure 2(d), when the sample is annealed at 370 °C for 10 min. The loss of the alloy-related contrast indicates that the surface alloy is thermally unstable during annealing.

Figures 3(a) and (b) show the evolution of the LEEM I–V characteristics during the course of the entire experiment. Prior to growing the surface alloy, we obtain an I–V measurement, shown in figure 3(b), from a terrace of the clean Cu(100) surface. Immediately after the growth of the surface alloy (0.4 ML Pd), a second I–V measurement is obtained from the terrace far from the step-overgrowth region. After the growth of the alloy, a peak has appeared in the I–V curve near 20.3 eV. Figure 3(a) shows how the intensity at 20.3 eV, I (20.3 eV), measured on a terrace, evolves over the course of the experiment. After annealing, an I–V measurement is acquired on a terrace. The peak at 20.3 eV associated with the surface alloy has vanished and the post-anneal I–V characteristics are similar to those of clean Cu, suggesting that Pd has diffused deeper into the Cu bulk.

3.2. LEEM I–V analysis of interdiffusion

A dynamical LEEM I–V analysis confirms that, during annealing, Pd is diffusing into the Cu bulk. Figure 4 shows the results of the analysis applied to the experimental results of figure 3. The optimized calculated I–V curves compare well with experiment. Prior to annealing, the optimized layer concentrations are $C_1 = (4 \pm 11)$ at.%, $C_2 = (38 \pm 10)$ at.%, and $C_3 = (0 \pm 16)$ at.%. Here, C_i denotes the concentration

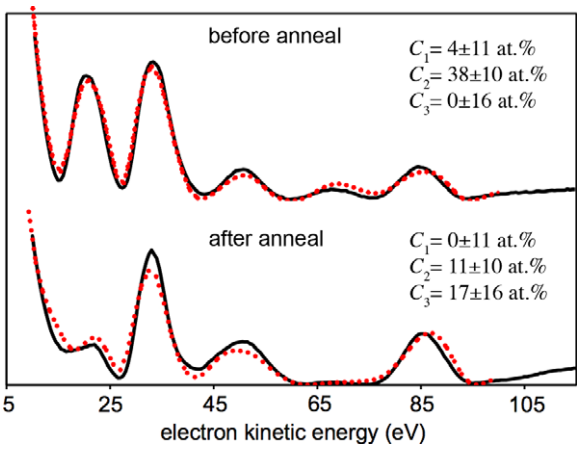

Figure 4. Experimental and optimized calculated LEEM I–V curves before annealing the 0.4 ML Pd alloy and after annealing at 370 °C for ∼10 min. Solid black lines are measured I–V curves and broken red lines are the optimized calculated I–V curves with the Pd concentrations, C_i, indicated.

of the ith atomic layer starting from the surface, $i = 1$. After annealing, the optimized concentrations are $C_1 = (0 \pm 11)$ at.%, $C_2 = (11 \pm 10)$ at.% and $C_3 = (17 \pm 16)$ at.% (see footnote 4). Following annealing, greater disparities are expected between the calculated and experimental curves due to intensity contributions from Pd in deeper atomic layers. After annealing, the second-layer Pd concentration has decreased, while the third-layer concentration has increased, demonstrating that Pd is diffusing into the Cu bulk.

3.3. Interdiffusion kinetics

We use the 20.3 eV LEEM intensity, I (20.3 eV), measured on a terrace to estimate the time dependence of the second-layer Pd concentration, $C_2(t)$. From $C_2(t)$, we estimate the rate of Pd diffusion into the Cu bulk using a simple one-dimensional random walk model for Pd tracer diffusion.

Figure 3(a) shows that, during Pd deposition, I (20.3 eV) grows in nearly direct proportion to the Pd dose. Under the conditions of our experiment, the Pd dose is rapidly and predominantly incorporated into the second atomic layer [11–13]. Therefore, during alloy *growth* the intensity at 20.3 eV is proportional to the second-layer Pd concentration, $C_2(t)$. During annealing, I (20.3 eV) drops again to a value near that measured on the clean surface. The Pd concentration prior to annealing is known from the LEED calibration of the Pd source. Using these conditions, we convert the 20.3 eV intensity to Pd concentration, $C_2(t)$. Figure 5(a) shows the time dependence, $C_2(t)$, for several temperatures in the range 250–370 °C.

The key distinction between the alloy *growth* and the *annealing* experiment is that, during annealing, Pd is incorporated into deeper layers below the surface. It is likely that the changing structure and Pd concentrations (C_3, C_4, etc) of deeper layers influence the evolution of the intensity at 20.3 eV. During the interdiffusion experiment, the most significant deviations from the assumed proportionality,

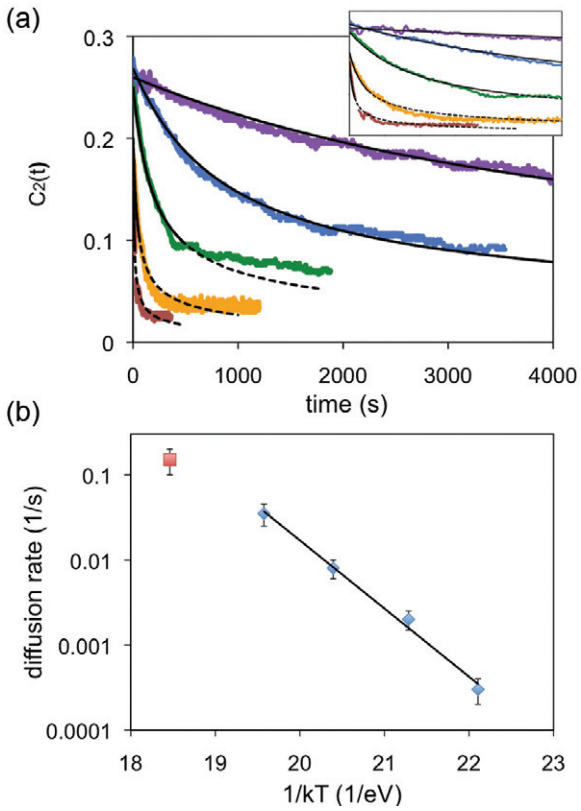

Figure 5. (a) The time dependence of the Pd concentration of the second layer estimated from the 20.3 eV electron intensity for $T = 248$, 272, 295, 320 and 370 ± 5 °C (top to bottom). Black smooth lines are fits to the experimental data using our diffusion model. The inset shows the first 600 s of the annealing process on an expanded timescale. (b) Temperature dependence of the diffusivities, D, obtained from the fits in (a). The Arrhenius relation gives $E_a = (1.8 \pm 0.6)$ eV, with a prefactor of $10^{13.5\pm1.5}$ s^{-1}. The larger red square data point at the highest temperature has been excluded because it is unlikely that the sample reached thermal equilibrium at the nominal thermocouple temperature during the relatively rapid annealing experiment.

$C_2 \sim I$ (20.3 eV), are caused by the changing structure and composition of the third atomic layer for two reasons. First, on the timescale of our measurements, a rapid and sizeable change in the Pd concentration occurs only in the third atomic layer, assuming a Gaussian evolution of the Pd concentration profile. Second, the attenuation length for 20 eV electrons in a metal is several ångströms, so we have decreasing sensitivity to variations in each successive atomic layer. We estimate the errors induced by changes in the composition of layer 3 using our dynamical I–V model[5]. Errors in $C_2(t)$ induced by the changing composition, ΔC_3, are small (∼10%) over a period during which I (20.3 eV) drops to 67% of the initial value at the start of the anneal. Although a strict proportionality $C_2(t) \sim I$ (20.3 eV) fails as the composition of deeper layers evolves, errors in $C_2(t)$ can be quantified and they are small over a sufficiently long interval at the outset of the interdiffusion measurement that the diffusion rate can be obtained.

[5] Uncertainty due to the change in C_3 is estimated by using I–V calculations to determine the partial derivative associated with ΔC_3 near the optimized value.

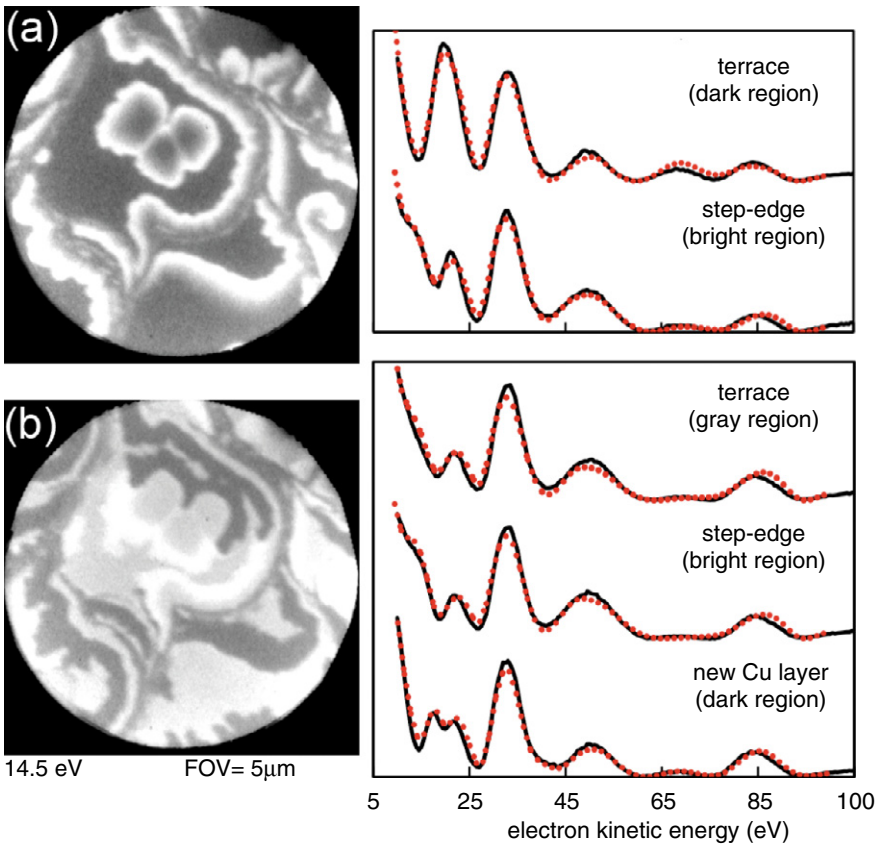

Figure 6. LEEM images and I–V analysis of the composition of the terraces and step-overgrowth regions of a 0.6 ML Pd surface alloy (a) after growth and (b) after the annealing at $T = 270\,^{\circ}\mathrm{C}$ for 30 min. Black solid lines represent measured I–V curves and red broken lines are the optimized calculated I–V curves.

We model Pd diffusion into the Cu bulk as a one-dimensional continuous-time random walk in which the surface is represented by a completely reflecting barrier. In our model, the Pd concentration is localized at the reflecting barrier at $x = 0$ at time $t = 0$. The Pd spreads into the bulk ($x < 0$) by a continuous-time random walk for $t > 0$. The model is implemented by a kinetic Monte Carlo simulation. The time evolution of the concentration at the reflecting barrier is fitted to the experimental $C_2(t)$ curves using the diffusion rate as a tunable fitting parameter. Figure 5(a) shows fits to $C_2(t)$ using our diffusion model. Our simple model gives accurate fits at lower temperatures (the two uppermost curves). At higher temperatures or longer times, as C_2 decreases, the influence of the changing composition of deeper layers is more significant. As the strict proportionality between $C_2(t)$ and I (20.3 eV) fails, we expect a divergence between our model and experiment. In consideration of such errors, we have fitted the experimental data only for $C_2(t) > 10\%$ as[6] indicated by solid lines. Broken lines show the subsequent model evolution of C_2.

To estimate the activation barrier to diffusion from the surface alloy into the Cu bulk, we plot the temperature-dependent diffusion rates in Arrhenius form in figure 5(b). A fit to the rates gives $D = 10^{13.5\pm1.5}\ \mathrm{s}^{-1}\ \exp[-(1.8 \pm 0.6)\ \mathrm{eV}/k_\mathrm{B}T]$. Within bulk single-crystal Cu, Pd impurities diffuse by exchange with bulk vacancies [14–17]. The activation barrier, E_a, for bulk-vacancy-mediated diffusion includes the sum of the bulk Cu vacancy formation and migration energies, as well as barrier modifications involved in the exchange between Pd and a bulk vacancy. Previous experimental studies have yielded values for E_a of 1.7 ± 0.2 eV [17] for polycrystalline samples and 2.12 eV (no stated uncertainty) to 2.37 ± 0.01 eV in single crystals [14–16].

[6] Over the range of the fits, we estimate uncertainty in the best-fit diffusion rates of the order of 20% due to a similar uncertainty in the value of C_2.

4. Structural evolution near step edges

After annealing over long time periods, all evidence of the surface alloy phase vanishes, both on the terraces and in the step-overgrowth regions. In the step-overgrowth region, we observe a more complex structural evolution *during* the anneal. At the high side of atomic steps, both the second and the third atomic layers contain significant concentrations of Pd due to the step-overgrowth mechanism observed by Hannon *et al* [12]. During the annealing, a new Cu layer nucleates and grows *on top* of the overgrowth region. Under this new layer of Cu, we observe the development of a layered structure resembling the fcc Cu_3Pd $L1_2$ bulk alloy phase [1, 18].

Figure 6(a) shows a 14.5 eV image of a 0.6 ML Pd surface alloy prior to annealing, along with I–V curves from the terrace and step edge. As before, dark regions contain

Table 1. Optimized structural parameters for the alloy surface for the I–V analysis described in figure 6. R_2 is the reliability factor minimized by optimizing alloy structural parameters. The C_i are the Pd concentrations for the ith layer and d_{ij} are the interlayer spacings between ith and jth layers. z_2 is the rippling in the second layer indicating the upward shifting of the Cu sublattice plane. Dashes indicate parameters that were not optimized in the analysis, but rather fixed at values characteristic of the Cu bulk.

	R_2	C_1 (at.%)	C_2 (at.%)	C_3 (at.%)	C_4 (at.%)	d_{12} (Å)	d_{23} (Å)	d_{34} (Å)	z_2 (Å)
Terrace before anneal	0.01	9 ± 11	50 ± 10	6 ± 16	—	1.85	1.84	—	0.07
Terrace after anneal	0.02	5	13	32	—	1.80	1.86	—	0.06
Step before anneal	0.01	15	18	35	—	1.81	1.84	—	0.09
Step after anneal	0.01	8	6	38	—	1.81	1.87	—	0.03
Cu_3Pd structure	0.02	4	20	8	44 ± 20	1.81	1.82	1.85	0.07

primarily second-layer Pd and brighter regions contain second- and third-layer Pd. The brighter structures near the center of the image are Cu adatom islands, which sometimes nucleate and grow during the growth of the surface alloy because Cu is ejected to the surface by Pd incorporation. Figure 6(b) shows the same terrace after annealing at 270 °C for 30 min. The brighter step-overgrowth regions in figure 6(b) are still evident. A new structure, which appears black in the images, has nucleated and grown *over* the bright step-overgrowth regions. This dark region is a new layer of Cu, surrounded by an atomic step, as determined by post-annealing deposition of additional Cu onto the surface. We believe that the new layer grows because Cu is liberated to the surface as the bulk and/or surface vacancy concentrations come up to equilibrium at the annealing temperature [20, 21].

To determine the near-surface composition under this new layer of Cu, we perform a LEEM I–V analysis. The optimized I–V curves for the surface alloy prior to annealing are shown in figure 6(a). Table 1 summarizes the parameters, and their optimized values, obtained in the I–V analysis. The Pd concentrations in the first three atomic layers on the terrace are $C_1 = (9 \pm 11)$ at.%, $C_2 = (50 \pm 10)$ at.% and $C_3 = (6 \pm 16)$ at.%. Near the step edge, the optimized concentrations are $C_1 = (15 \pm 11)$ at.%, $C_2 = (18 \pm 10)$ at.% and $C_3 = (35 \pm 16)$ at.%. Figure 6(b) shows the optimized LEEM I–V curves after annealing. On the terrace, the concentrations have dropped to $C_1 = (5 \pm 11)$ at.%, $C_2 = (13 \pm 10)$ at.% and $C_3 = (32 \pm 16)$ at.%. In the bright step overgrowth, at the step edge, we find $C_1 = (8 \pm 11)$ at.%, $C_2 = (6 \pm 10)$ at.% and $C_3 = (38 \pm 16)$ at.%.

In the dark region where the new Cu layer has grown, the optimized Pd concentrations are $C_1 = (4 \pm 11)$ at.%, $C_2 = (20 \pm 10)$ at.%, $C_3 = (8 \pm 16)$ at.% and $C_4 = (44 \pm 20)$ at.%. In this layered structure, Pd resides primarily in 2×2 fcc sublattices of the second and fourth layers, separated by layers of relatively pure Cu. This structure resembles the ordered fcc Cu_3Pd $L1_2$ bulk alloy phase shown in figure 1(c). At the temperatures (200–370 °C) and Pd volume concentrations of our experiments, the Cu_3Pd $L1_2$ structure is the expected bulk alloy phase [18]. In our experiment, we estimate the volume concentration of Pd, shared amongst the first four atomic layers, to be 16 at.%. Below 370 °C, Pd–Cu bulk alloys with 8–21 at.% are observed to have the Cu_3Pd $L1_2$ structure [18].

At higher temperatures and/or longer annealing times, e.g. in the 370 °C anneal described in figures 2 and 3, this Cu_3Pd $L1_2$ phase also becomes dilute and undetectable. After the anneal, described in figures 2 and 3, there is no evidence of the step-edge contrast or the ∼18 eV double-peak I–V feature, as in figure 6, associated with the Cu_3Pd $L1_2$ phase.

5. Summary

We have used LEEM to show how the evolution of a surface alloy phase can be used to track the bulk interdiffusion of Pd into Cu. This technique is very likely applicable to a variety of binary, or more complex, alloy systems. Although alloying by bulk interdiffusion, and more specifically alloying in the Pd–Cu alloy system, has been thoroughly explored previously, LEEM, combined with a dynamical LEEM I–V analysis, allows the unique capability to observe and quantify the process in real-time, layer by atomic layer, at the nanometer scale.

Acknowledgments

We thank J B Hannon of IBM, and N C Bartelt, P J Feibelman, R Stumpf and B S Swartzentruber of Sandia National Labs, for insightful discussions. Work performed at Sandia was supported by the US DOE, Office of BES, DMSE. Sandia is operated by Sandia Corporation, a Lockheed Martin Company, for the US DOE's NNSA under contract no. DE-AC04-94AL85000. Work at UNH was supported by the Petroleum Research Fund under grant no. 46323-AC5.

References

[1] Woodruff D (ed) 2002 *Surface Alloys and Alloy Surfaces* (Amsterdam: Elsevier)
[2] Bose A C (ed) 2009 *Inorganic Membranes for Energy and Environmental Applications* (New York: Springer)
[3] Hu C-K, Rosenberg R and Lee K Y 1999 *Appl. Phys. Lett.* **74** 2495
[4] Park C W and Vook R K 1993 *Thin Solid Films* **226** 238
[5] Bussmann E *et al* in preparation
[6] Murray P W, Stensgaard I, Laeagsgard E and Besenbacher F 1996 *Surf. Sci.* **365** 591
[7] Graham G W, Schmitz P J and Thiel P A 1990 *Phys. Rev.* B **41** 3353
[8] Andersen G W, Jensen K O, Pope T D, Griffiths K, Norton P R and Schultz P J 1992 *Phys. Rev.* B **46** 12880
[9] Andersen G W, Pope T D, Jensen K O, Griffiths K, Norton P R and Schultz P J 1993 *Phys. Rev.* B **48** 15823
[10] Koymen A R, Lee K H, Yang G, Jensen K O and Weiss A H 1993 *Phys. Rev.* B **48** 2020
[11] Barnes C J, AlShamaileh E, Pitkänen T, Kaukasoina P and Lindroos M 2001 *Surf. Sci.* **492** 55

[12] Hannon J B, Sun J, Pohl K and Kellogg G L 2006 *Phys. Rev. Lett.* **96** 246103
[13] Sun J, Hannon J B, Kellogg G L and Pohl K 2007 *Phys. Rev.* B **76** 205414
[14] Petersen N L 1963 *Phys. Rev.* **132** 2471
[15] Philofsky E M and Hilliard J E 1969 *J. Appl. Phys.* **40** 2198
[16] Butrymowicz D B, Manning J R and Read M E 1976 *J. Phys. Chem.* **5** 103 Ref. Data http://www.nist.gov/srd/PDFfiles/jpcrd76.pdf
[17] Jeon I J, Hong J H and Lee Y P 1994 *J. Appl. Phys.* **75** 7825
[18] Subramanian P R and Laughlin D E 1991 *J. Phase Equilib.* **12** 231
[19] Van Hove M A and Tong S Y 1979 *Surface Crystallography by LEED* (Berlin: Springer)
[20] McCarty K F, Nobel J A and Bartelt N C 2001 *Nature* **412** 622
[21] Poelsema B, Hannon J B, Bartelt N C and Kellogg G L 2004 *Appl. Phys. Lett.* **84** 2551